Minimum Variability Time Scales of Long and Short GRBs

G. A. MacLachlan[1]⋆, A. Shenoy[1], E. Sonbas[2,3], K. S. Dhuga[1], B. Cobb[1],
T. N. Ukwatta[1,2,4], D. C. Morris[1,2,5], A. Eskandarian[1], L. C. Maximon[1],
and W. C. Parke[1]

[1] *Department of Physics, The George Washington University, Washington, D.C. 20052, USA.*
[2] *NASA Goddard Space Flight Center, Greenbelt, MD 20771, USA.*
[3] *University of Adiyaman, Department of Physics, 02040, Adiyaman, Turkey.*
[4] *Department of Physics and Astronomy, Michigan State University, East Lansing, MI 48824, USA.*
[5] *Department of Physics, University of Virgin Islands, Virgin Islands, USA.*

24 January 2012

ABSTRACT
We have investigated the variability of a sample of long and short Fermi/GBM Gamma ray bursts (GRBs) using a fast wavelet technique to determine the smallest time scales. The results indicate different variability time scales for long and short bursts in the source frame and that variabilities on the order of a few milliseconds are not uncommon. The data also indicate an intriguing relation between the variability scale and the burst duration.

Key words: Gamma-ray bursts

1 INTRODUCTION

The prompt emission from Gamma-ray Bursts (GRBs) shows very complicated time profiles that hitherto elude a satisfactory explanation. Fenimore & Ramirez-Ruiz (2000) reported a correlation between variability of GRBs and the peak isotropic luminosity. The existence of the variability-luminosity correlation suggests that the prompt emission light curve is embedded with temporal information related to the microphysics of GRBs. Several models have been proposed to explain the observed temporal variability of GRB lightcurves. Leading models such as the internal shock model (reference) and the photospheric model (reference) link the rapid variability directly to the activity of the central engine. Others invoke relativistic outflow mechanisms to suggest that local turbulence amplified through Lorentz boosting leads to causally disconnected regions which in turn act as independent centers for the observed prompt emission. In more recent models, both Morsony et al. (2010) and Zhang & Yan (2011) argue that the temporal variability may show two different scales depending on the physical mechanisms generating the prompt emission.

In order to further our understanding of the prompt emission phase of GRBs and to explicitly test some of the key ingredients in the various models it is clearly important to extract the variability for both short and long gamma-ray bursts in a robust and unbiased manner. It is also clear

that the chosen methodology should not only be mathematically rigorous but also be sufficiently flexible to apply to transient phenomena for multiple temporal resolutions and a wide dynamic range.

In this paper, we extract variability time scales for GRBs using a method based on wavelets. The layout of the paper is as follows: the source of the data is described in section 2; the main aspects of the wavelet methodology are outlined in section 3; in section 4 we provide the details of the data analysis; in section 5 we present and discuss our main findings; finally, in section 6, we summarize our conclusions.

2 DATA

The Gamma-Ray Burst Monitor (GBM) on board Fermi observes GRBs in the energy range 8 keV to 40 MeV. The GBM is composed of 12 thallium-activated sodium iodide (NaI) scintillation detectors (12.7 cm in diameter and by 1.27 cm thick) that are sensitive to energies in the range 8 keV to 1MeV, and two bismuth germinate (BGO) scintillation detectors (12.7 cm diameter by 12.7 cm thick) with energy coverage between 200 keV to 40 MeV. The GBM detectors are arranged in such a way that they provide a full view of the sky (Meegan et al. 2009).

In this work, we have extracted light curves for the GBM NaI detectors over the entire energy range (8 keV - 1 MeV, also including the overflow beyond 1 MeV). Typically, the brightest three NaI detectors were chosen for the
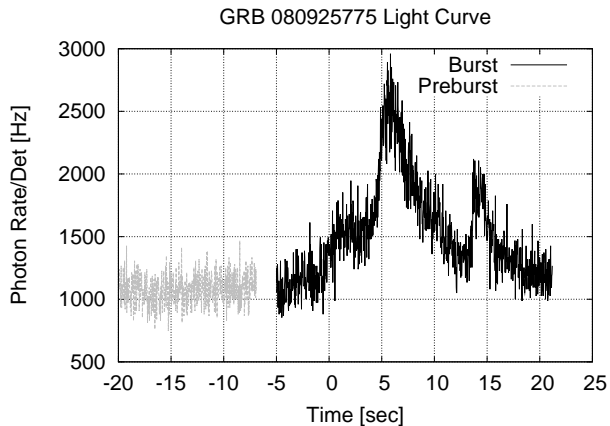
⋆ E-mail: maclach@gwu.edu (GAM)

Figure 1. GBM GRB080925775. Preburst portion of the light curve, used for background removal, is shown in gray. The burst portion, from which a time scale is extracted, is shown in black.

extraction. Lightcurves for both long and short GRBs were extracted at a time binning of 200 microseconds. The long GRBs were extracted over a duration starting from about 15-20 seconds before the trigger (pre-burst) and up to about 50 seconds after the T_{90} for the burst (post-burst) without any background subtraction. For short GRBs, the pre- and post-burst regions were chosen to be about 10 seconds each. The T_{90} durations were obtained from the GCN circulars distributed by the GBM team and directly from the literature.

3   METHODOLOGY

We report on our model-independent statistical investigation of the variability of Fermi/GBM long and short GRBs. We extract this information by using a fast wavelet transformation to encode GRB light curves into a wavelet representation and a statistical measure of the variance of wavelet coefficients is computed over multiple time-scales.

3.1   Minimum Variability Time Scales

It is often the case when multiple processes are present that one process will dominate the others at certain time scales but those same processes may exchange dominance at other time scales. A wavelet technique is useful in these situations because the variances of wavelet coefficients are sensitive to whichever processes dominate the light curve at a given time scale. Moreover, the technique can be used to classify those dominant processes as well as provide a means to determine the characteristic time scale, τ_β, for which the processes exchange dominance. Determination of τ_β is useful for the development of theoretical models and the understanding of observational data. Indeed, such a transition time scale sets a lower bound beyond which it is not meaningful to look for high frequency, small time scale variability.

3.2   Wavelet Transforms

Wavelet transformations have been shown to be a natural tool for multi-resolution analysis of non-stationary time-series (Flandrin 1989, 1992; Mallat 1989). Wavelet analysis is similar to Fourier analysis in many respects but differs in that wavelet basis functions are well-localized, *i.e.* have compact support, while Fourier basis functions are global. Compact support means that outside some finite range the amplitude of wavelet basis functions goes to zero or is otherwise negligibly small (Percival 2000).

3.2.1   Discrete Dyadic Wavelet Transforms

In principle, a wavelet expansion forms a faithful representation of the original data, in that the basis set is orthonormal and complete. Given the discrete nature of the data, we employ a discrete wavelet analysis The rescaled-translated nature of the wavelet basis functions make the wavelet transform well-localized in both frequency and time, which results in an insensitivity to polynomial backgrounds for photon counts. The level of insensitivity, formally known as the vanishing moment condition, can be adjusted by choice of wavelet basis function. By construction, the discrete wavelet transform is a multi-resolution operation (Mallat 1989). Such wavelets, denoted $\psi_{j,k}(t)$, form a dyadic basis set, i.e. wavelets in the set have variable widths and variable central time positions.

The wavelet analysis employed in this study, as with the fast Fourier transform, begins with a light curve with N elements,

$$X_i = \{X_0 \dots X_{N-1}\}, \tag{1}$$

where N is an integer power of two. The light curve is convolved with a scaling function, $\phi_{j,k}(t_i)$, and wavelet function, $\psi_{j,k}(t_i)$ which are rescaled and translated versions of the original scaling and wavelet functions $\phi(t_i) = \phi_{0,0}$, and $\psi(t_i) = \psi_{0,0}$. Translation is indexed by k and rescaling is indexed by j. The rescaling and translation relation is given by

$$\psi_{j,k}(t) = 2^{-j/2}\psi(2^{-j}t - k). \tag{2}$$

The precise forms of the scaling and wavelet functions are not unique. The choices are made according to the features one wishes to exploit (Percival 2000; Addison 2002). The scaling function acts as a smoothing filter for the input time-series and the wavelet function probes the time-series for detail information at some time scale, Δt, which is twice that of the finest binning of the data, T_{bin}. In the analysis, the time scale is doubled

$$\Delta t \to 2\Delta t$$

and the transform is repeated until

$$\Delta t = NT_{bin}.$$

In this analysis we choose the Haar scaling/wavelet basis because it has the smallest possible support, has one vanishing moment, and is equivalent to the Allan variance determination, allowing a straightforward interpretation.

3.2.2   The Haar Wavelet Basis

Convolving X with the scaling functions yields approximation coefficients,

$$a_{j,k} = \langle \phi_{j,k}, X \rangle. \tag{3}$$

Interrogating X with the wavelet basis functions yields scale and position dependent detail coefficients,

$$d_{j,k} = \langle \psi_{j,k}, X \rangle, \tag{4}$$

It is interesting to point out that for the trivial 2×2 case the Haar wavelet transform and the Fourier transform are identical.

3.3 Logscale Diagrams and Scaling

Logscale diagrams are useful for identifying scaling and noise regions. Construction of a logscale diagram for each GRB proceeds from the variance of detail coefficients Flandrin (1992),

$$\beta_j = \frac{1}{n_j} \sum_{k=0}^{n_j - 1} |d_{j,k}|^2, \tag{5}$$

where the n_j are the number of detail coefficients at a particular scale, j. A plot of $\log_2$ variances versus scale, j, takes the general form

$$\log_2 \ \beta_j = \alpha j + \text{constant}, \tag{6}$$

and is known as a logscale diagram. A linear regression is made of each logscale diagram and the slope parameter, α, (depicting a measure of scaling) is estimated. White-noise processes appear in logscale diagrams as flat regions while scaling processes appear as sloped regions with the following condition on the slope parameter, $1 \leqslant \alpha \leqslant 3$, coming about from the fact that the fractal dimension of the data must range from one to two.

4 DATA ANALYSIS

4.1 Analysis of Long and Short GRBs

4.1.1 Background Subtraction

Background subtraction in a wavelet-based analysis of time scale dependent variances should remove noise variability from the light curve while allowing physical variability arising from the GRB to remain for further analysis. Background subtraction for a statistical analysis of variability via wavelet transforms should proceed in the space variances as opposed to a traditional flat or linear subtraction of counts. This owes to the fact that Haar detail coefficients are insensitive to polynomial trends in the signal up to first order. Subtraction of a flat or linear background from a light curve is an operation under which the wavelet transform is invariant (as are Fourier transforms) apart from the mean signal coefficient.

The GRB light curves show power at various variablity time scales. Most often, there is a region of the logscale diagram (log-power verses log-varibility time) with a single slope, indicating scaling in the power over those variability-times, and a flat region at the shortest variability times, indicating the presence of white-noise. Some of this white-noise may be intrinsic to the GRB. Some may be attributed to background emissions from the sources not including the GRB in question. We therefore express the variability of

the burst, β_j^{burst}, at time scales j as comprising of individual variances: a scaling component, $\beta^{scaling}$; an intrinsic noise component, β^{noise}; and a background component, $\beta^{background}$. The variability of the burst can then be described as a linear combination of the component variances so long as the components have vanishing covariances. In this event we write,

$$\beta_j^{burst} = \beta_j^{scaling} + \beta_j^{noise} + \beta_j^{background}. \tag{7}$$

The minimum variability time scale is identified from a logscale diagram by the octave closest to the intersection of the flat intrinsic noise domain, β_j^{noise}, with the sloped scaling domain, $\beta_j^{scaling}$. It is at this time scale that a structured physical process appears to give way to one that is stochastic and unstructured. Clearly one seeks to remove $\beta_j^{background}$ from Eq. 7 to arrive at the cleanest possible signal,

$$\beta_j^{burst} \to \beta_j^{clean} \equiv \beta_j^{burst} - \beta_j^{background} = \beta_j^{scaling} + \beta_j^{noise}. \tag{8}$$

In order to estimate the variance of the background during the burst, we will assume that the variance obtained from a preburst portion of the light curve can serve as an acceptable surrogate for the background variance. That is,

$$\beta_j^{preburst} \equiv \beta_j^{background}, \tag{9}$$

and then the background is removed from the signal according to the relation,

$$\log_2(\beta_j^{clean}) = \log_2(\beta_j^{burst} - \beta_j^{preburst}). \tag{10}$$

A simple algebraic manipulation of Eq. 10 gives a form,

$$\log_2(\beta_j^{clean}) = \log_2(\beta_j^{burst}) + \log_2\left(1 - \frac{\beta_j^{preburst}}{\beta_j^{burst}}\right). \tag{11}$$

For long GRBs, the preburst is defined relative to a 0 s trigger time as -20 s to -5 s and for short GRBs the preburst is defined to be from -15 s to -1 s.

4.2 Simulation

The efficacy of this background subtraction method was tested using simulated data in the form of fractional Brownian motion (fBm) time series which were first discussed by Mandelbrot (1968). The fBms were combined with Poisson noise. The numerical computing environment MATLAB was used to produce 1000 realizations of fBms with scaling parameter α randomly chosen from the range $1.0 \leqslant \alpha \leqslant 2.0$ by using a uniform random number generator. The fBms were combined with a Poisson noise with variance, λ_1, randomly chosen from the range $0.25 \leqslant \lambda_1 \leqslant 1.0$ by using a uniform random number generator. This Poisson noise is regarded as intrinsic to the GRB. The fBms and the Poisson noises thus produced were combined and stored as *ideal* light curves, shown in green on the left panel of Fig. 2. The logscale diagrams obtained from the ideal light curves are used to compare against the results of the subtraction procedure.

Another set of Poisson noise with variances, λ_2, were randomly chosen from the range $1.0 \leqslant \lambda_2 \leqslant 4.0$ by using a uniform random number generator. These noise signals are interpreted as external *background* meant to be removed by the subtraction procedure and are shown in black on the left panel of Fig. 2.
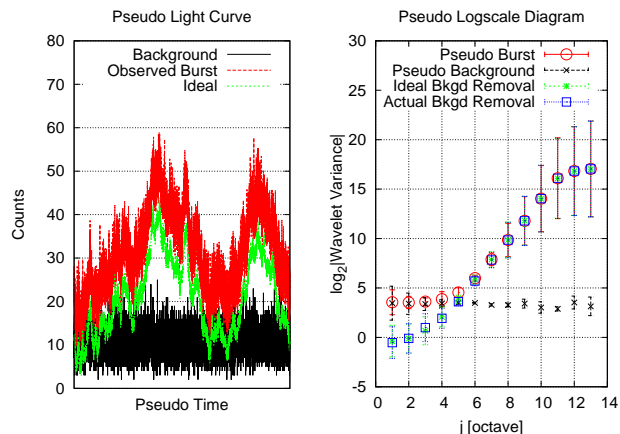
Figure 2. In the left hand panel are simulated lightcurves and noise processes: an *ideal* fBm process (green) and a *background* Poisson noise (black). The sum of the fBm and Poisson processes is shown in red and is labeled *observed*. The *observed* light curve (red) is the sum of the fBm and Poisson noise. The right hand panel shows the results of the background subtraction procedure. Red and black points show the logscale diagrams for the *observed* lightcurve *background*, respectively. The green data shows the logscale diagram for the *ideal* lightcurve and the blue data are the logscale with background removed. The agreement between green and blue data demonstrates the merit of the background removal procedure.

The ideal light curves were then combined with external backgrounds resulting in pseudo-*observed* light curves shown in red on the left panel of Fig. 2. The pseudo-observed light curves and the external background noises were transformed into wavelet coefficients and wavelet variances were computed according to Eq. 5. The variances of the pseudo-observed light curve (labeled *actual*) and the background are plotted in the right panel of Fig. 2 in red and black, respectively. The background was subtracted from the pseudo-observed light curve as detailed in Eq. 2 and the resulting corrected variances are plotted in blue in the right panel of Fig. 2. The corrected variances are to be compared to the variances of the ideal light curve which are plotted in green. Notice the close agreement between the background-subtracted variances and the variances of the ideal light curve. The pseudo data shown in Fig. 2 is one realization out of the 1000 that were generated but is representative of the set.

In summary, 1000 simulated light curves were generated and background noise was added. The light curves with background noise were then denoised using the same algorithm applied to actual GRB data in which preburst data were used as a surrogate for background. The simulated background subtracted variances were then compared to the variances of the ideal light curves, i.e., light curves without external background noise. The results indicate that the background subtraction method is robust and gives confidence that external background noise can be subtracted from the GRB light curves with the assumption that preburst data can serve as a surrogate for background noise.
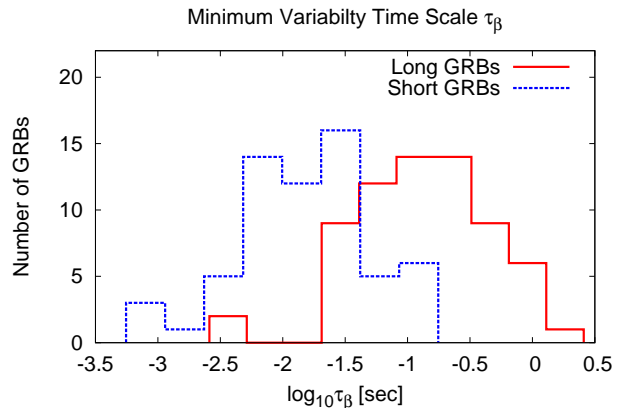

Figure 3. A histogram of minimum variability time scales, in the observer frame, for long and short GRBs. Note that logarithmic scale on the temporal axis. It is clear that long distribution is displaced from the short distribution.

4.3   Selection Criteria

We began by examining 66 short GRBs and 67 long GRBs for a first-pass analysis of τ_β and the results are shown in Fig. 3. For the second-pass we require a brightness cut, i.e., that the variance of the burst be greater than twice the variance of the preburst for at least one octave,

$$\frac{\beta_j^{burst}}{\beta_j^{preburst}} > 2. \tag{12}$$

This reduced the sample to 33 short GRBs (Tab. 1) and 66 long GRBs (Tab. 2) for a total of 99 and it is these GRBs which are used to create Fig. 4 and Fig. 7. For the third-pass through the data we require the same brightness cut in Eq. 12 as well as there be a known z and that a source frame t_{90} had been tabulated in Gruber et al. (2011). In addition, we also required that the first order poynomial fits to the noise region and to the scaling region each had a χ^2/d.f. that was less than 2. This cut further reduced the data set to 2 short GRBs and 18 long GRBs for a total of 20 GRBs. These 20 GRBs that meet the selection criteria for the third and final pass are given in Tab. 3 and were used to created Fig. 5 and Fig. 6.

4.3.1   Circular Permutation

Spurious artifacts due to incidental symmetries resulting from accidental misalignment (Percival 2000; Coifman 1995) of light curves with wavelet basis functions are minimized by circularly shifting the light curve against the basis functions. Circular shifting is a form of translation invariant denoising (Coifman 1995). It is possible a shift will introduce additional artifacts by moving a different symmetry into a susceptible location. The best approach is to circulate the signal through all possible values, or at least a representative sampling, and then take an average over the cases which do not show spurious correlations.
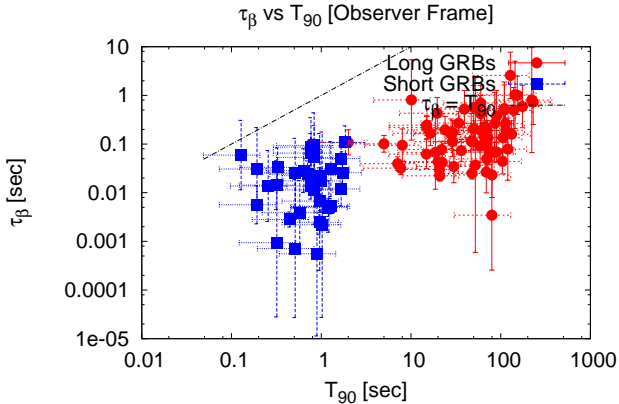
Figure 4. Minimum variability time scale versus GCN T_{90}. In many cases uncertainties for GCN T_{90}s are unknown and so a relative uncertainty of 62% has been applied to each T_{90}.

Figure 5. Minimum variability time scale versus Gruber et al. (2011) T_{90}.

4.3.2 Reverse-Tail Concatenation

Both discrete Fourier and discrete wavelet transformations imply that the expansion is periodic, with a repeat period equal to the full time range of the input data. This can be interpreted to mean that for a series of N elements, $\{X_0, X_1 \ldots X_{N-1}\}$ then X_0 is made a surrogate for X_N and X_1 is made a surrogate for X_{N+1}, and so forth. This assumption may lead to trouble if X_0 is much different from X_{N-1}. In this case, artificially large variances may be computed. Reverse-tail concatenation minimizes this problem by making a copy of the series which is then reversed and concatenated onto the end of the original series resulting a new series with a length twice that of the original. Instead of matching boundary conditions like,

$$X_0, X_1, \ldots, X_{N-1}, X_0, \qquad (13)$$

we match boundaries as,

$$X_0, X_1, \ldots X_{N-1}, X_{N-1}, \ldots, X_1, X_0. \qquad (14)$$

Note that the series length has thus artificially been increased to $2N$ by reversing and doubling of the original series. Consequently, the wavelet variances at the largest scale in a logscale diagram reflect this redundancy. This is the reason the wavelet variances at the largest scale are excluded from least-squares fits of the scaling region.

Another difficulty in wavelet expansions is that the intialization procedure of the multi-resolution algorithm may pollute the detail coefficients at the finest scale (see Strang and Nguyen 1997; Abry et al. 2003). For this reason we follow the advice of Abry et al. (2003) and discard the detail coefficients at the finest scale.

Figure 6. Minimum variability time scales versus Gruber et al. (2011) T_{90} with symbol size determined by Luminosity. One notices that no relation between minimum variability time scale, T_{90}, and luminosity is apparent.
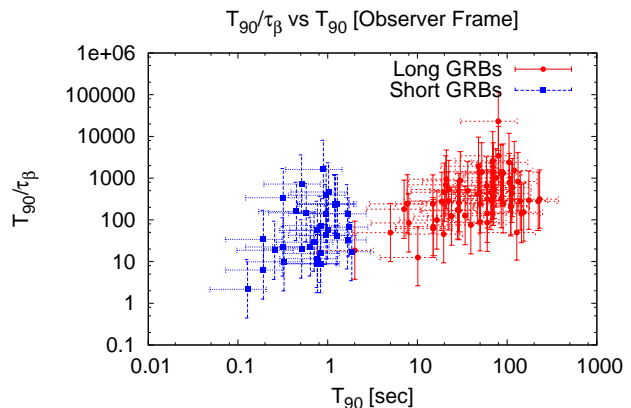
Figure 7. The ratio duration to minimum variability time scale (GCN T_{90} to τ_β) vs. duration (GCN T_{90}).

5 RESULTS AND DISCUSSION

For a large sample of short and long GBM bursts, we have used a technique based on wavelets to determine the minimum time scale (τ_β) at which scaling processes dominate over random noise processes. The τ_β values, along with the GRB names, luminosities and the known redshifts are listed in Table 1. The τ_β is the intersection of the scaling region
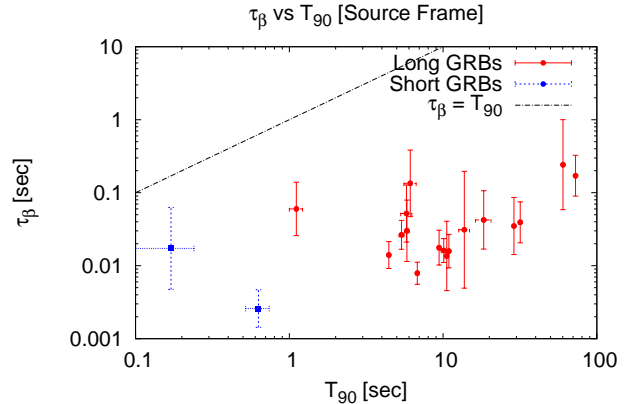
(red-noise) of the spectrum in the logscale diagram with that of the flat portion representing the (white-noise) random noise component. We interpret this transition as a measure of some physical process, intrinsic to GRB production, whose highest frequency is still resolvable from white noise. Histograms of the extracted τ_β values for long and short GRBs are shown in Fig. 3. We make two observations regarding these histograms: There is a clear temporal offset in the extracted mean τ_β values for long and short GRBs. We believe this is the first clear demonstration of this temporal difference. Walker et al. (2000), who studied the temporal variability of long and short bursts using the BATSE data set did not report a systematic difference between the two types of bursts. The two histograms are quite broad and very similar in dispersion. While the difference in the mean τ_β is understandable (a point we discuss further elsewhere) the similarity of the dispersion is somewhat surprising since the progenitors and the environment for the two types of bursts are presumably very different. The comparison is qualitative at best however because the τ_β scale has not been corrected for redshift (z), an effect that impacts the long bursts more than the short bursts. In passing we note that the dispersion of the τ_β histogram (for long bursts) is in agreement with the results of Ukwatta et al. (2011) who performed a power density spectral analysis of a large sample of Swift long GRBs. In that work the authors extracted threshold frequencies and related them to a variability scale.

In Fig. 4 we show a log-log plot of τ_β versus T_{90} (the duration of the bursts); long GRBs are indicated by circles, the short ones by squares and both time scales are with respect to the observer frame. As in the histograms above, the fact that short GRBs, in general, tend to have smaller τ_β values compared to long GRBs, is evident in this figure. Also shown in the figure (as a dash line) is the trajectory of τ_β equal to T_{90}. We note that no (long) GRBs exhibits an τ_β longer than T_{90} although interestingly a few short GRBs of extremely short duration appear to be approaching the limit of equality. In addition to establishing a characteristic time scale for short and long bursts, this figure also hints at a positive correlation between this time and the duration of bursts. We note that the τ_β scale spans approximately two decades for both sets of GRBs and that the two groups are fairly well clustered in the τ_β-T_{90} plane. A closer examination of the two groups, however, indicates that a correlation between τ_β and T_{90}, if present, is marginal at best. This is certainly true for the short-GRB group, especially given the large uncertainties in the T_{90}s for these bursts. The situation for the long-burst group on the other hand is not immediately clear. In order to explore this further we cast the τ_β and the T_{90} time scales into the source frame by applying the appropriate $(1+z)$ factor to the GRBs for which the z is known. Unfortunately the z is not available for the majority of the short GBRs but we note that the correction is the same for both axes and is, to first order, small for the short GRBs since the mean z for this group is < 0.5. The corrected results for long-GRBs are shown as a log-log plot in . We see from this figure the appearance of a very intriguing feature: A plateau region in which the τ_β is essentially independent of T_{90} and a scaling region in which the τ_β appears to increase with T_{90}, with the transition occurring around T_{90} approximately equal to 10 seconds.

If one assumes a positive correlation between luminosity and variability as suggested by a number of authors, then one might expect smaller τ_β values for higher luminosity bursts compared to those of lower luminosity. To investigate this, the data (in Fig. 5) are re-plotted in Fig. 6 which the size of each datum symbol has been modulated by the luminosity of the burst, i.e., a large symbol implies a high luminosity and a small symbol a low luminosity. We see from Fig. 6 that such a connection between τ_β and luminosity is not evident.

Under the assumption that the τ_β is a measure proportional to the smallest causally-connected structure associated with a GRB lightcurve, it is then possible to interpret the scaling trend in terms of the internal shock model in which the basic units of emission are assumed to be pulses that are produced via the collision of relativistic shells emitted by the central engine. Indeed, we note that Quilligan et al. (2002) in their study of the brightest BATSE bursts with $T_{90} > 2$ sec explicitly identified and fitted distinct pulses and demonstrated a strong positive correlation between the number of pulses and the duration of the burst. In our work we have not relied on identifying distinct pulses but instead have used the multi-resolution capacity of the wavelet technique to resolve the smallest temporal scale present in the prompt emission. If the smallest temporal scale is made from pulse emissions from the smallest structures, then we can get a measure of the number of pulses in a given burst through the ratio T_{90}/τ_β . In the simple model in which a pulse is produced every time two shells collide then the ratio, T_{90}/τ_β, should show a correlation with the duration of the burst. A plot of this ratio versus T_{90} is shown for a sample of short and long bursts in Fig. 7. The correlation is apparent.

It is now widely accepted that the progenitors for the two classes of GRBs are quite distinct i.e., the merger of compact objects in the case of short GRBs and the collapse of rapidly rotating massive stars in the case of the GRBs. Formation of an accretion disk in the two cases is posed in a number of models but important factors such as the size of the disk, the mass of the disk, the strength of the magnetic field, in addition to the magnitude of the accretion rate during the prompt phase, remain largely uncertain. With contributions from intrinsic variability of the central engine or nearby shock-wave interactions within a jet, we should not be surprised to observe a systematic difference in the extracted variability time scales for long and short bursts, since the progenitors have different spatial scales. Knowing the variability timescales, we can estimate the size of an assumed emission region. From Fig. 4, we note that the smallest temporal-variability scale for the short bursts is approximately 3 ms and that for the long bursts is approximately 30 ms: These times translate to emission scales of approximately 10^8 and 10^9 cm respectively. Our variability times and size scales are generally consistent with the findings of Walker et al. (2000) although these authors also reported observing time scales as small as few microseconds. We find no evidence for variability times as low as a few microseconds.

Morsony et al. (2010) modeled the behavior of a jet propagating through the progenitor and the surrounding circumstellar material and showed that the resulting lightcurves exhibited both short-term and longterm variability. They attribute the long-term variability, at the scale of

few seconds, to the interaction of the jet with the progenitor. The short-term scale, at the level of milliseconds, they attribute to the variation in the activity of the central engine itself. Alternatively, Zhang & Yan (2011) consider a model in which the prompt emission is the result of a magnetically powered outflow which is self-interacting and triggers rapid turbulent reconnections to power the observed GRBs. This model also predicts two variability components but interestingly and in contrast to the findings of Morsony et al. (2010) , it is the slow component that is associated with the activity of the central engine, and the fast component is linked to relativistic magnetic turbulence. While we are not in a position to distinguish between these two models it is intriguing nonetheless to note (see Fig. 4) that indeed there do appear to be two distinct time domains for the τ_β: a plateau region dominated primarily by short bursts although it includes some long bursts too, and a scaling region (i.e., correlated with duration) that is comprised solely of long bursts. In addition, we observe that the time scale in the plateau region is the order of milliseconds whereas that for the scaling region is approaching seconds.

There is considerable dispersion in the extracted τ_β. The variation is evident for both short and long-duration GRBs. The main cause of this dispersion is not fully understood but one factor that may play a significant role is angular momentum. As Lindner et al. (2010) note, the basic features of the prompt emission can be understood in terms of accretion that results via a simple ballistic infall of material from a rapidly rotating progenitor. Material with low angular momentum will radially accrete across the event horizon whereas the material with sufficient angular momentum will tend to circularize outside the innermost stable circular orbit and form an accretion disk. Simulations that go beyond the simple radial infall model (Lindner et al. 2010, 2011) suggest that the formation of the disk leads to an accretion shock that traverses outwards through the infalling material. If one assumes that the initiation of such an accretion shock and the subsequent emission of the prompt gamma-rays are associated with a particular time scale, the variability of this scale then (as given by the dispersion in τ_β for example) presumably reflects the different dynamics (initial angular momentum and the mass of the black hole) of each GRB in our sample. In the case of long GRBs, the mass of the central black hole can vary by an order of magnitude thus potentially explaining a large part of the dispersion seen in the τ_β. However a similar dispersion for short bursts is difficult to reconcile using the same arguments since the mass range for the central black hole in standard merger models (at least for NS-NS mergers) is expected to be significantly smaller.

6 CONCLUSIONS

We have studied the temporal properties of a sample of prompt-emission ligfhtcurves for short and long-duration GRBs detected by the Fermi/GBM mission. By using a technique based on wavelets we have extracted the variability timescales for these bursts. Our main results are summarized as follows:

a) Both short and long-duration bursts indicate a temporal variability at the level of a few milliseconds. Variability

of this order appears to be a common feature of GRBs. This finding is consistent with the work of Walker et al. (2000). However, unlike these authors we do not find evidence of variability at a time scale of few microseconds.

b) In general the short-duration bursts probe a variability time scale that is significantly shorter than long-duration bursts. In addition, the τ_β values seem not to depend in any obvious way on the luminosity of the bursts. The dispersion over different GRBs in the extracted time scale for short-duration bursts is an order of magnitude within the smallest variability time, that time being approximately 3 milliseconds. The dispersion for the long-duration bursts is somewhat larger. The origin of the dispersion in either case is not known, although we should expect that the size of the initial angular momentum and the mass of the system play significant roles.

c) For short-duration bursts, the variability parameter τ_β shows negligible dependence on the duration of the bursts (characterized by T_{90}). In contrast, the long-duration bursts indicate evidence for two variability time scales: a plateau region (at the shortest time scale) which is essentially independent of burst duration and a scaling region (at the higher time scale) that shows a positive correlation with burst duration. The transition between the two regions occurs around T_{90} of approximately 10 seconds in the source frame.

APPENDIX

Table 1. Analyzed Short GRBs

GRB	T_{90}[sec]	τ_β [sec]
080723913	0.192	0.0307
080802386	0.576	0.0039
080815917	0.832	0.0532
080831053	0.864	0.0000
080905499	0.960	0.0067
080919790	0.896	0.0006
081012045	1.216	0.0052
081024245	0.960	0.0224
081102365	1.728	0.0258
081105614	1.280	0.0306
081107321	1.664	0.0504
081115891	0.320	0.0009
081119184	0.128	0.0592
081209981	0.192	0.0057
081213173	0.256	0.0138
081216531	0.768	0.0138
081226044	0.832	0.0936
081230871	0.512	0.0256
090108020	0.704	0.0241
090120627	1.856	0.1081
090126245	0.960	0.0025
090206620	0.320	0.0143
090227772	1.280	0.0053
090228204	0.448	0.0028
090303542	0.512	0.0007
090308734	1.664	0.0120
090331681	0.832	0.0114
090427644	1.024	0.0022
090429753	0.640	0.0285
090510016	1.199	0.0049
090520832	0.768	0.0868
090531775	0.768	0.0653
090927422	0.995	0.0175
100117879	0.326	0.0331

Table 2. Analyzed Long GRBs

GRB	T_{90}[sec]	τ_β [sec]	GRB	T_{90}[sec]	τ_β [sec]	GRB	T_{90}[sec]	τ_β [sec]	GRB	T_{90}[sec]	τ_β [sec]
80723557	105	0.044	81007224	10	0.0026	90323002	132.1	0.1598	90810659	230	0.7319
80723985	60	0.1894	81008832	144.4	1.029	90328401	90	0.0682	90814950	120	0.0787
80724401	75	0.074	81009140	49.3	0.1095	90411991	18.7	0.0673	90829672	85	0.0678
80727964	79.7	0.0035	81009690	50	0.5603	90419997	90	0.3728	90831317	69.1	0.0266
80804972	19.6	0.4306	81101532	8	0.0948	90423330	10.1	0.808	90902462	21	0.0223
80806896	60	0.4189	81125496	15	0.2182	90424592	48	0.0249	90926181	20	0.0435
80807993	80	0.0232	81129161	59	0.0912	90425377	72	0.1346	90926914	109.7	0.5373
80810549	106	0.1353	81207680	153	1.002	90516137	140	0.4938	91003191	20.7	0.03
80816503	70	0.1067	81215784	7.7	0.0319	90516353	221.8	0.7992	91020900	39.4	0.5226
80817161	70	0.1919	81221681	34	0.2701	90519881	52.2	0.0369	91024372	109.8	0.4988
80825593	22	0.0775	81222204	24	0.1956	90528516	68	0.1314	91127976	7.1	0.0395
80905705	128	2.5761	81224887	50	0.2055	90618353	113.2	0.2631	91208410	14.9	0.0621
80906212	5	0.1011	81231140	29	0.1124	90620400	16.5	0.1667	100414097	22.3	0.0418
80916009	66	0.2266	90102122	30	0.0347	90626189	70	0.0498	100814160	174.5	0.5908
80916406	60	0.6995	90117632	86	0.2674	90717034	70	0.1881	100816026	2	0.1082
80925775	29	0.1748	90131090	36.4	0.0733	90718762	28	0.1621	100906576	114.4	0.192
80928628	46.9	0.1141	90202347	66	0.1444	90809978	15	0.2436			

Table 3. Analyzed Final GRBs. GCN Circ. 8100, GCN Circ. 9057, GCN Circ. 9415, GCN Circ. 9406, GCN Circ. 10204, GCN Circ. 10595, GCN Circ. 111245

Number	T_{90}[sec]	δT_{90}[sec]	τ_β[sec]	τ_β^-[sec]	τ_β^+[sec]	logLum	logLum$^-$	logLum$^+$
080804972[1]	6.120	0.560	0.1344	0.0470	0.3843	52.5539	52.4768	52.6401
080810549[2]	13.750	1.100	0.0311	0.0049	0.1966	52.9818	52.9196	53.0362
080916009[3]	18.370	2.130	0.0424	0.0169	0.1064	54.0170	53.9786	54.0523
081222204[1]	5.780	0.480	0.0519	0.0211	0.1275	53.1004	53.0755	53.1206
090102122[5]	10.560	0.270	0.0136	0.0046	0.0407	52.9395	52.9106	52.9666
090323002[1]	28.910	0.130	0.0350	0.0142	0.0861	53.837	52.5051	53.8642
090328401[2]	31.740	0.580	0.0393	0.0206	0.0750	52.2529	52.217	52.279
090424592[3]	10.100	0.390	0.0161	0.0111	0.0235	52.2095	52.1987	52.2227
090510016[5]	0.630	0.110	0.0026	0.0014	0.0047	52.42	52.3282	52.5694
090618353[3]	72.660	0.450	0.1709	0.0897	0.3253	51.9279	51.8633	51.945
090902462[5]	6.800	0.110	0.0079	0.0056	0.0112	53.7701	53.7629	53.7772
090926181[5]	4.440	0.060	0.0140	0.0092	0.0214	53.8692	53.8606	53.8777
091003191[1]	10.910	0.160	0.0158	0.0093	0.0269	52.6561	52.619	52.7147
091127976[2]	5.370	0.200	0.0265	0.0168	0.0418	51.5682	51.5517	51.5805
091208410[1]	5.820	0.190	0.0301	0.0114	0.0793	52.1614	52.1146	52.2541
100117879[1]	0.170	0.070	0.0173	0.0047	0.0629	53.2504	53.2475	53.2533
100414097[2]	9.420	0.210	0.0177	0.0102	0.0306	53	52.9253	53.0318
100814160[3]	60.250	0.900	0.2421	0.0585	1.0024	51.9175	51.8537	51.9523
100816026[2]	1.110	0.110	0.0600	0.0258	0.1391	51.8555	51.8301	51.8862

REFERENCES

Abry, P., et al. 2003, *Self-similarity and long-range dependence through the wavelet lens*, Theory and Applications of Long-Range Dependence, Boston: Birkhauser, 527-556

Addison P. S. 2002, Fractals and Chaos: An Illustrated Course, Institute of Physics Publishing

Coifman R. R. and Donoho D. L. 1995, Translation-invariant de-noising, Springer-Verlag, 125–150

Fenimore, E. E., & Ramirez-Ruiz, E. 2000, arXiv:astro-ph/0004176

Flandrin P. 1989, IEEE, Transactions on Information Theory, 11, 674–693

Flandrin P. 1992, IEEE, Transactions on Information Theory, 38, 910–917

Gruber, D. et al. 2011, arXiv:1104.5495 [astro-ph.HE].

Lindner, C. C., Milosavljevic, M., Couch, S. M., & Kumar, P. 2010 *ApJ.*, 713, 800

Lindner, C. C., Milosavljevic, M., Shen, R., & Kumar, P. 2011, arXiv:1108.1415v1 [astro-ph.HE]

Mallat S. G. 1992, IEEE, Transactions on Pattern Analysis and Machine Intelligence, 11, 674–693

Mandelbrot, B. B. and Van Ness, J. W. 1968, SIAM Review, 10, 422-437

Meegan, C. et al. 2009, *ApJ.*, 702, 791

Morsony, B. J., Lazzati, D., & Begelman, M. C. 2010, arXiv:1002.0361

Percival, D. B. and Walden, A. T. 2002, Wavelet Methods for Time Series Analysis, Cambridge University Press

Quilligan, F., et al. 2002, *A.& A.*, 385, 377

Strang, G. and Nguyen, T. 1997, *Wavelets and filter banks*, Wellesley-Cambridge Press

Ukwatta, T. et al. 2011, *MNRAS*, 412, 875

Walker, K. C., et al. 2000 *ApJ.*, 537, 264

Zhang, B., & Yan, H. 2011, ApJ, 726, 90